Cross-scales Analysis Of Shear Behavior In Fontainebleau Sandstone

Trung-Kien Nguyen[1*] and Thanh-Trung Vo[2,3]

[1] Faculty of Building and Industrial Construction, Hanoi University of Civil Engineering, Hanoi, Vietnam
[2] School of Transportation Engineering, Danang Architecture University, Danang city, Vietnam
[3] Office of Research Administration, Danang Architecture University, Danang city, Vietnam
[*] Corresponding author. E-mail: kiennt3@huce.edu.vn

Received: December 28, 2023; Accepted: April 21, 2024

Modeling the behavior of sandstone across the scales is a crucial subject of numerous research studies. Since the material is composed of smaller grains, its macroscopic mechanical behavior is thus dominant by the microscopic evolutions of the constituents. In this paper, a cross-scale model (CSM) intimately combines Finite Element Method (FEM), and Discrete Element Method (DEM) was developed. At the sample scale, FEM is used while DEM is employed to model grains' interactions. Cross-scale simulation is then performed showing good correlation between numerical and experimental data on Fontainebleau sandstone. Remarkably, going down to the scale of material constituent, the result suggests that the shear band observed at sample scale are directly connected to the microscopic manifestation at grains scale. Three zones corresponding to the sample failure level are highlighted. Those are the core of SB where the material degrades the most, the adjacent zones where material are partly damaged and quasi-intact zones outside the SB. Microscopic properties in terms of void ratio and cohesive coordination number vary consistently with the identified zones.

Keywords: Cross-scales analysis; Macro-micro; Shear band; Sandstone

http://dx.doi.org/10.6180/jase.202503_28(3).0002

1. Introduction

Unlike purely frictional granular materials (for instance dry sand), cohesive-frictional granular materials are characterized by the presence of a cohesion that prevents relative displacement between particle constituents. Within the family of cohesive granular materials, cemented granular materials are of "strongly" cohesive type. Many natural or industrial granular materials are cemented granular materials, such as sedimentary rocks (e.g., sandstones) or building materials (e.g., concrete). These materials consist of a dense granular assembly with cement joints connecting the particles and partially or totally filling the pore space. This cemented bond translates into tensile, shear and rolling strengths. When subjected to loading, they exhibit highly complex behavior due to complicated microstructure and particle-based interactions.

In the field of rock mechanics, various localized patterns have been observed in rock sample [1, 2]. They are usually classified into shear band (SB), deformation band or combined shear failure. Among them, shear band investigations have received much attention by both field/laboratory experiments and numerical tests [3–10]. The formation of SB in rock samples has been investigated by several works in which the occurrence and development of SB are related to the possible degradation of cemented bond inside such material.

In laboratory experiments on sandstone, degradation of material strength by cracking is observed. Cracking occurs on several scales: on grain level those are inter-granular or intra-granular cracks, which are characterized by bond broken; on a macroscopic laboratory scale, these coalescence of micro-cracking lead to macro-cracks which divide the sample into several blocks and causing discontinuity in the material. The failure of sandstone at multiple scales was

experimentally and numerically observed in the works of [8, 9, 11–13]. In these works, they observed that a highly degraded zone was observed inside the SB and leading to the overall failure of the specimen.

The onset and development of shear band can be theoretically analyzed by the bifurcation theory [14, 15] or numerically with suitable constitutive laws by pure Finite Element Method (FEM). Such phenomena can also be treated by pure discrete models such as the case of Discrete Element Method (DEM). Despite such progress, the relationship between failure at different scales is still elusive. And it is not clear how can we consider the degradation of multiple scales and connect between them. Thus, the aim of this paper is to deal with these issues from a cross-scale viewpoint. This is also our attempt to identify key micro-mechanisms and their role in triggering the SB in soft sandstone. To this end, a cross-scale model (CSM) that intimately combines FEM and DEM is used. This latter originally developed during the works of [16, 17], will be enhanced by adopting an advanced and fully cohesive for DEM part. A fully bonded model is represented that can describe the cohesion nature existing between grain inside sandstone microstructure. This cross-sale analysis is believed to better describe the complex behavior of failure in cemented geomaterials by multi-scale viewpoints. After the introduction, the paper is organized as follows: section 2 introduces the methodology background including basic FEM, DEM equations and cross-scale model (CSM) principle. The main results illustrating the calibration of numerical model against existing experimental data is then given in section 3. Further analysis about the degradation characteristics of the materials is also discussed in the same section. The paper ends with some concluding remarks in section 4.

2. Cross-scales model (CSM)

2.1. Finite Element background

For equilibrium state, the virtual principle reads:

$$\int_V \sigma : \delta D dV = \int_S t \cdot \delta v dS + \int_V f \cdot \delta v dV \tag{1}$$

Where σ is the Cauchy stress, δv is an arbitrary function which can be imagined to be a virtual velocity field. V is the space volume; t is the surface traction at any point of boundary S and f body force per unit of considered volume. Taking the finite element discretization procedures leads to solving the equation system as follows.

$$Ku = F \tag{2}$$

Where K and F are the stiffness matrix and nodal forces vector; u is the unknown displacement vector of finite element nodes. For non-linear material behavior such as the case of geomaterials, solving non-linear system Eq. (2) required the use of iterative procedure such as Newton-Raphson method. In such case, the stiffness matrix K is generally determined from the shape function of finite element and consistent tangent operator C of material constitutive law. The consistent tangent operator (CTO) is defined as follows:

$$C = \frac{d\sigma}{dh} \tag{3}$$

Where σ is the Cauchy stress and $h_{ij} = \partial x_i / \partial x_j$ is the deformation gradient. For DEM-based constitutive model, the operator C can be numerically or analytically determined based on granular assembly characteristics.

2.2. DEM-based constitutive law

A specific in-house DEM routine was developed in order to build a constitutive law. The procedure is performed on a granular assembly (called Volume Element - VE) composed of grains. To be able to describe a constitutive law, the DEM routine is specifically designed to obtain the corresponding Cauchy stress (σ) when deformation gradient (h) is applied to the VE. The DEM procedure is based on classical DEM, originally proposed by Cundall and Strack [18]. The DEM integration procedure is based on the third predictor-corrector scheme [19]. In the granular assembly, grains interacts via a fully model for cemented granular materials that incorporates the normal (f_n^c), tangential (f_t^c) and rolling (M^c) bonds [20, 21]. The failure surface is illustrated in Fig. 1(c) and also depend on the exponential coefficient n_f. The bonding is broken once the rupture criterion is beyond the failure surface as defined in Eq. (4).

$$\varsigma = \frac{f_n}{f_n^c} + \left(\frac{f_t}{f_t^c}\right)^{n_f} + \left(\frac{M}{M^c}\right)^{n_f} \leq 1 \tag{4}$$

In the rupture criterion, the normal contact force (f_n) is proportional to the normal deflection via normal stiffness k_n; the tangential contact force (f_t) is based on Coulomb friction law via tangential stiffness k_t and intergranular friction coefficient μ. The rolling resistance is involved in such a manner that we consider contact length between interacting grains. By this way, the contact can transmit a moment (M) which is calculated based on rolling stiffness k_r and relative rotation of pair of grains in contact. Once bond is broken, the contact becomes purely frictional with rolling resistance. Details equations on contact model and DEM integration process are given in [21].

As a summary the DEM-based constitutive law consist of the following parameters, mainly divided into two groups: (i) VE properties involve grain size, number of grains, initial coordination number (number of contacts

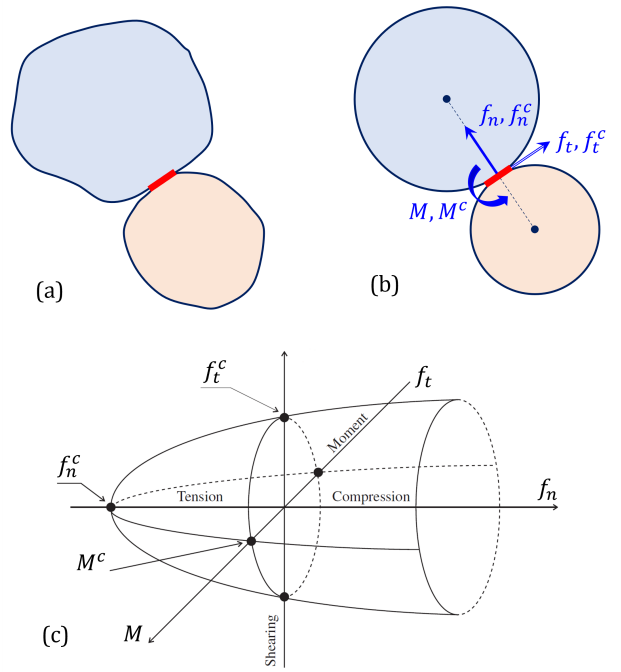

Fig. 1. Grain-grain contact model: (a) real grains in contact; (b) idealized grains in contact and (c) bond model.

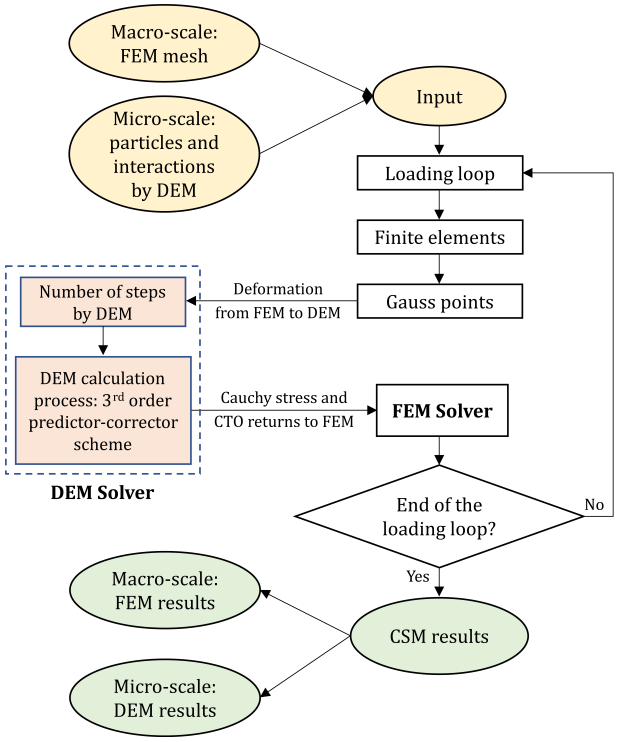

Fig. 2. CSM implementation algorithm.

per grain), grains' positions, void ratio; and (ii) contact law properties involve $k_n, k_t, k_r, f_n^c, f_t^c$ and M^c.

2.3. CSM principle and numerical implementation

The cross-scale model (CSM) is obtained by implementing the DEM-based constitutive model in a finite element code. The procedure consists in integrating a DEM-type numerical behavior law in place of the analytical behavior laws classically used in finite element codes. It involves several modifications to the original finite element code. The DEM code replaces the constitutive routine called at each integration point (Gauss point), which returns stress in response to a deformation gradient increment. This deformation gradient increment comes from the displacement field of the structure in the current state at the Gauss point under consideration. The numerical specific DEM routine code is also defined to returns a numerical evaluation of the consistent tangent operator C, as defined in Eq. (3). The algorithm of the cross-scale model is described in Fig. 2.

3. Cross-scale modeling of fontainebleau sandstone

To investigate the behavior of sandstone and microscopic origin of macroscopic failure, in this section we first calibrate our model with experimental data on Fontainebleau soft sandstone, provided by [10]. Once the calibration is performed, the advantage of cross-scale model is used to assess the multiple-scales analysis and their reciprocal relationship.

3.1. Cross-scale model

We aim to calibrate the numerical behavior with experiment result on Fontainebleau sandstone (FBS02 test in the ref. [10]), performed at 7 MPa of confining pressure (σ_3).

The parameters of DEM-based constitutive law are determined based on experimental data. This consists in determining the micro-parameters that will enable the calibration tests supplied, to be reproduced correctly. These micro-parameters are the stiffness level κ, the ratio between normal and tangential stiffness k_n/k_t, intergranular friction μ, the normal f_n^c, tangential f_t^c and rotational M^c strengths, and the exponent coefficient n_f. Moreover, the constitution of the particle assembly itself also plays a role, depending on the initial void ratio and average number of contacts per particles (also known as coordination number). In fact, depending on whether the VE is dense or loose, and whether the coordination number is greater or lesser, the dilatancy/contracting response will be different; and also, the softening induced by the progressive rupture of cohesive bridges between grains, leading to irreversible degradation.

To achieve this calibration task, the DEM-based consti-

tutive parameters are selected as follows: regarding VE characteristic, grain-size distribution and medium grain size $\langle a \rangle$ are similar to real material (i.e. Fontainebleau sandstone). The number of particles inside VE is 400. The VE is preloaded to 7MPa of isotropic stress. At this state, the granular VE exhibits dense packing as observed by [10]. The average coordination number of the VE is 3.05, meaning that a dense sample with intermediate coordination number is obtained (see Fig. 3). Other parameters involved in contact law are adjusted to better fit experimental curve notably the material strength, the cohesion and the friction. Specifically, the cohesion and stiffness are calibrated to ensure a compromise between the material strength and peak-stress of simulation result. Calibrated micromechanical parameters are summarized in Table 1. It should also be noted that this set of parameters may only be applicable to the investigated material in this paper. If we want to model other types of granular material, the calibration task must be performed correspondingly.

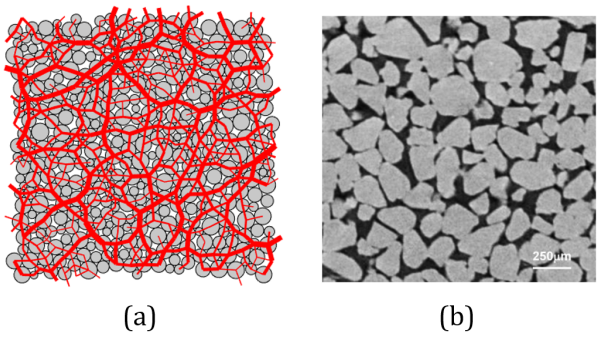

Fig. 3. Snapshot of VE (a) and microstructure of Fontainebleau sandstone (b) at 7MPa of isotropic compression [10]. In the VE, red lines connect center of particles in contact and representing the normal force intensity by its width.

The numerical CSM of the biaxial compression test is schematically illustrated in Fig. 4, consisting of two steps: first preloaded VE at isotropic compression 7MPa is assigned in every Gauss point of the mesh and then deviatoric loading by increasing of the vertical displacement (Fig. 4(a)), while keeping constant the confining pressure $\sigma_3 = 7MPa$. The macro mesh of the sample is discretized in 5×10 quadrilateral Q8 finite elements with 8 nodes and 4 Gauss points each.

3.2. Numerical results and discussions

3.2.1. Stress-strain macroscopic curves and strain localization

The macroscopic response of CSM is compared directly with the available experimental data presented in ref.

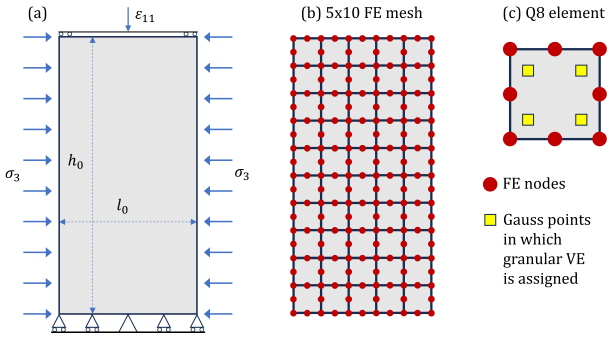

Fig. 4. FE model of 2D plane strain biaxial test: (a) boundary conditions, (b) Finite Element (FE) mesh and (c) Q8 element.

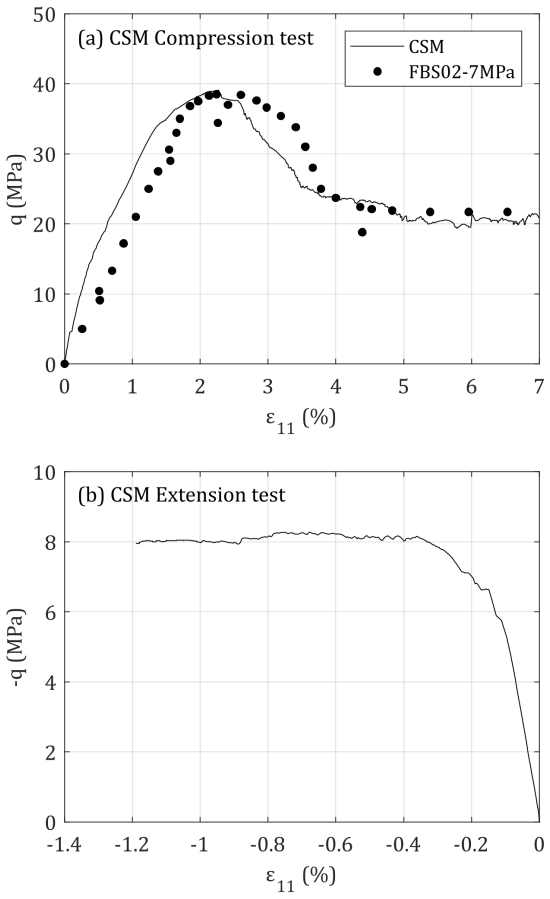

Fig. 5. CSM macro results: Biaxial compression (a) and extension (b) responses.

[10] in terms of deviatoric stress and vertical strain $(q = \sigma_1 - \sigma_3, \varepsilon_{11})$ relationship, as shown in Fig. 5(a). The (q, ε_{11}) curves show good agreement between the obtained and reference data. Both numerical and experimental curves reach peak at the same axial strain value

Table 1. Table 1. Micromechanical parameters.

	Parameters	Value
$k_n/(\sigma_0 \times \langle a \rangle)$	Normal stiffness	750
k_n/k_t	Stiffness ratio	1
k_r	Rolling stiffness	$\mu \times 10^{-1} \times \langle a \rangle$
μ	Friction coefficient	0.5
$f_n^c/(\sigma_0 \times \langle a \rangle)$	Normal bond	6
$f_t^c/(\sigma_0 \times \langle a \rangle)$	Tangential bond	6
$M^c/(\sigma_0 \times \langle a \rangle)$	Rolling bond	$6 \times \mu \times 10^{-1} \times \langle a \rangle$
n_f	Rupture criterion factor	2

($\varepsilon_{11} \approx 2.2\%$) with a deviatoric stress value $q_{\max} \approx 38MPa$, and then descend towards the same stress plateau $q_p \approx 20MPa$. At the initial hardening phase, it should be noted that the CSM curve gives a steeper stiffness than the experiment. It may be due to the use of perfect circular grains in the granular assembly VE. A biaxial extension simulation is also simulated by the CSM. The extension test concept is similar to the biaxial compression test. The only difference is that the top surface is pulled up instead of compressed. The response from this biaxial extension simulation is shown in Fig. 5(b). It is clearly seen that the curve is non-linear from the start of extension $\varepsilon_{11} = 0.1\%$, and rapidly tends towards a stress plateau. Similar observations were also obtained by [8].

Besides the consistent curves between numerical and experimental data, we now go further in quantitatively evaluate this comparison. In rock mechanics, the Mohr-Coulomb criterion is widely used for determining characteristic mechanical properties of the material. In this criterion, failure is modeled by the equation $\tau = \sigma_n \tan\varphi + c$, with two intrinsic parameters: the macroscopic cohesion c and the angle of internal friction φ; where σ_n is the normal stress and τ the shear stress. To get a clearer picture of the experimental and simulated material characteristics, we plot Mohr's circles in the stress plane (σ_n, τ) and then determine the corresponding material parameters, c and φ. From the Mohr's circles (Fig. 6), we can determine the cohesion and friction angle of the materials. Numerical simulations provided (C, φ)=(2.94MPa, 40°). The average parameters (C, φ) obtained from the experimental tests is (C, φ)=(3.00MPa,40°). Comparing these two sets of parameters shows that the numerical calculations almost give results which are the averages of the experimental tests. These results therefore show a very good comparison between experimental and numerical results in terms of material characteristics.

Regarding the deformation of the sample, as discussed in the introduction, SB is often seen to occur when sandstone sample is subjected to loading. In our case, deformation localization occurs in both experimental and numerical

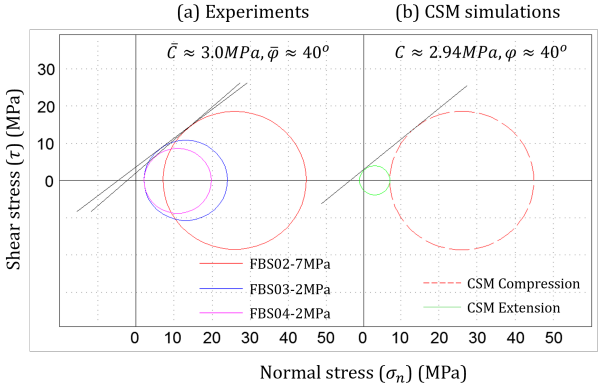

Fig. 6. Mohr-Coulomb circles.

cases. The shear bands observed in the experiment show an orientation of about 50° with respect to the horizontal axis. A SB is also obtained in numerical simulation. It is oriented approximately 51° with respect to the minor principal axis, i.e. the horizontal axis. Fig. 7 shows the deformed structure and the map of the von-Mises deformation at different instants $\varepsilon_{11} = 1\%, \varepsilon_{11} = 4\%$ and $\varepsilon_{11} = 7\%$ showing the formation and development of the SB. It can be seen that the SB is progressively developed and is well consistent with experimental observations. However, it should be noted that at FEM level, classical first gradient model is used, and once localization occurs, mesh dependency is observed. That's why in this CSM simulation, the thickness of SB is controlled by the finite element mesh size. The orientation of SB confirms again the quite good calibration of numerical CSM against experimental data.

3.2.2. Insight macroscopic shear band

In this section, we go inside into microscopic behavior of the SB. It is well known that when SB occurs, the sample is no longer homogeneous but structurally affected by the localized deformation. Macroscopically, it can be seen that the deformed mesh inside-, close-to- and outside- the SB are totally different. By approaching the center of SB, the finite element is more distorted showing that a com-

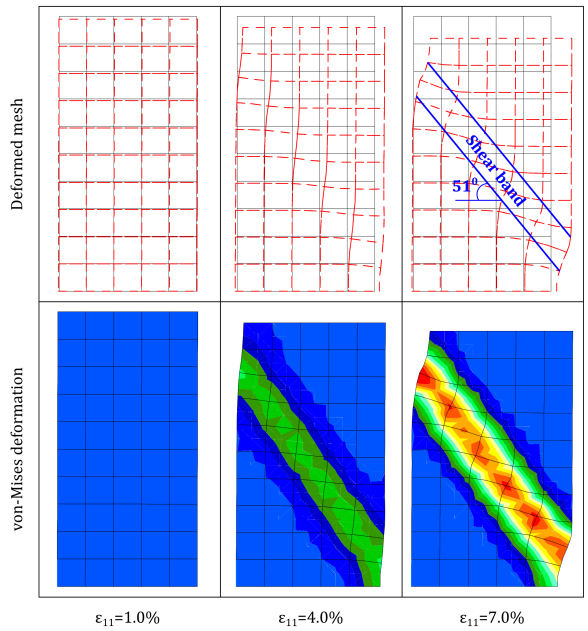

Fig. 7. Shear deformation of finite element mesh: top - initial mesh (continuous black line) and deformed mesh (dashed red line); bottom - Von-Mises deformation plotted on the deformed configuration.

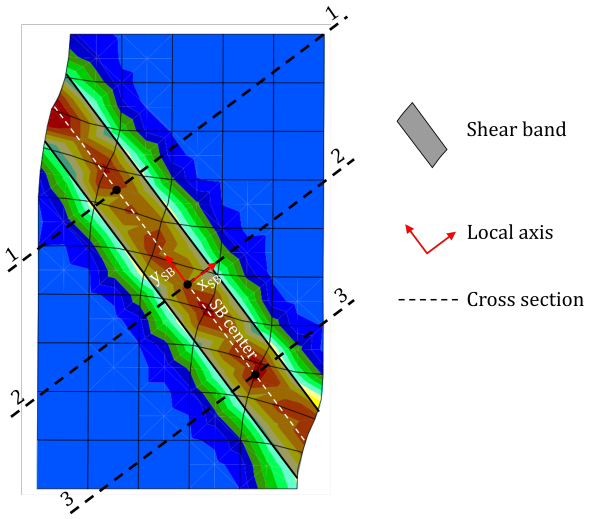

Fig. 8. Micro analysis with respect to the SB: three sections (1-1, 2-2 and 3-3) that perpendicular to the SB axis are considered.

bined shear-compression or shear-tension effects are dominant. These macro-observations are necessary reflected in micromechanical behavior such as void ratio or cohesive coordination number. As an advantage compared to conventional approach, the CSM exceptionally provides a straightforward manner to assess the behavior at multiple scales by studying at macro-finite element mesh and at the Gauss point level where microscopic information is located.

To perform micro-analysis insight the macro-behavior, different cross-sections are considered as depicted in Fig. 8. The three cross-sections are perpendicular to the SB axis, they pass through elements inside and outside the SB. We now plot the variation of micro properties in terms of void index and cohesive coordination number of VE, along the cross-section with respect to the local axis of the SB. The void ratio is defined as the volume of void divided by the volume of solid and cohesive coordination number is the average cohesive number of contacts per grains within the VE.

From Figs. 9 and 10, it is noticed that the void ratio and cohesive coordination number strongly depends on their location to the SB center axis. Higher void ratio and smaller cohesive coordination number are found inside the SB. The void ratio reaches a maximum value of 0.3 inside the SB (zone I) and rapidly (but not suddenly) decreases toward a value close to the initial outside the SB (zone III). There is also a transition zone (zone II) where microscopic properties are intermediate between those inside and outside the band. This means that we obtain here dilating SB in the current simulation. Moreover, as the loading progresses, the finite element inside SB are subjected to complicated loading (shear-compression combination), leading to the rupture of intergranular bond (open or slip of cohesive contacts). This is in agreement with experimental observation by micro-tomography performed by [9, 10].

From the results, three zones can be distinguished based on the distance to the center of the SB where clear difference in terms of cracking phenomenon and void ratio is highlighted. The shear zone is characterized by the high cracking intensity of cemented bond.

4. Conclusions

In this paper, a CSM in which DEM-based constitutive law is integrated into FEM calculations has been introduced. At DEM-level, fully cemented model was used for grain-grain interactions. The model has successfully produced the macro-behavior, the onset and orientation of shear band in soft Fontainebleau sandstone. The good comparison between experimental and numerical prediction provides capabilities of the developed model in investigating the behavior of cemented granular materials. The consistent results were shown in terms of macroscopic responses, Mohr-coulomb criterion parameters (cohesion and friction angle)

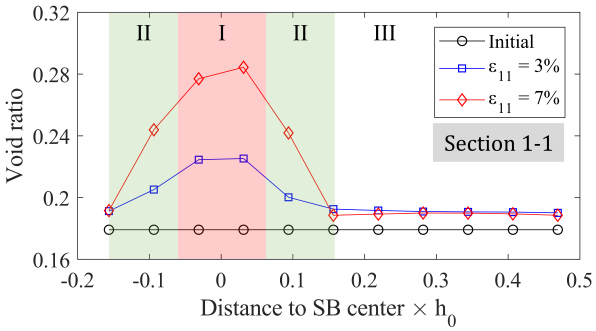

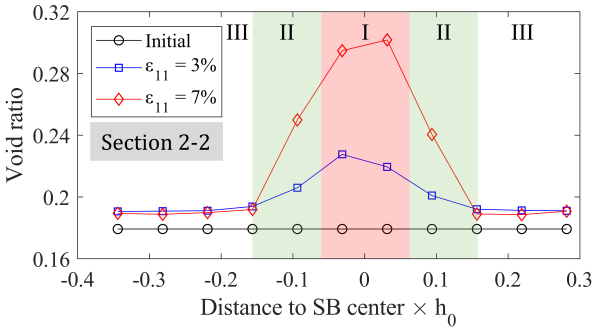

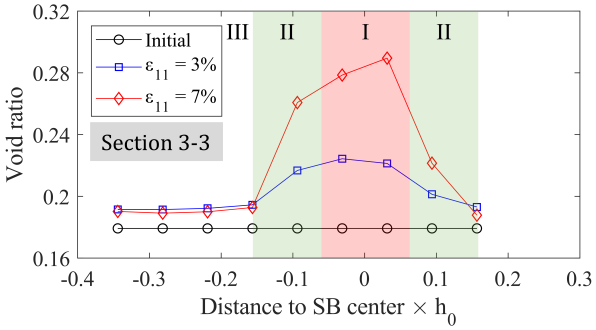

Fig. 9. Void ratio variation across the SB: I – Core of the SB; II – Adjacent zones to the SB; III – Outside the SB. The distance to the SB center is the local coordinate xSB as defined in Fig. 8

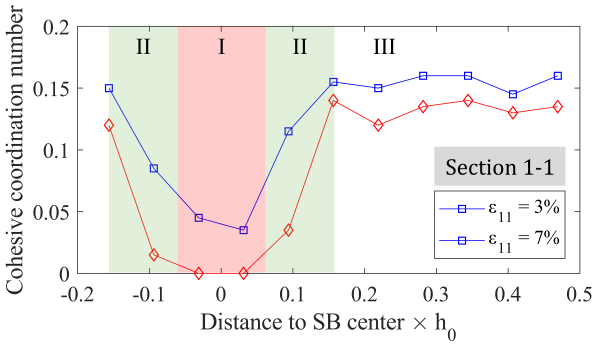

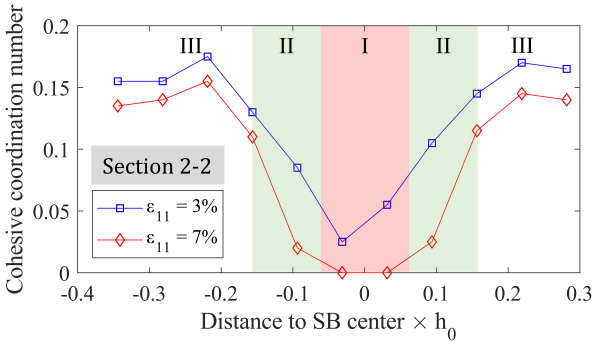

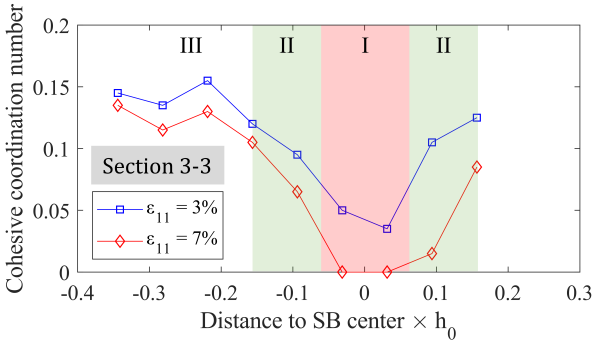

Fig. 10. Cohesive coordination number variation across the SB: I – Core of the SB; II – Adjacent zones to the SB; III – Outside the SB. The distance to the SB center is the local coordinate xSB as defined in Fig. 8

and shear banding orientation. Moreover, thanks to the numerical results, we observed that the localization of deformation in form of SB is associated with micro-cracking at grain level, which was experimentally observed in [9, 10].

For the class of geomaterials like sandstone, the behavior of materials is controlled by interactions at smaller scales and micro-mechanism evolutions. Thus, powerful numerical tools are required to assess the behavior at multiple scales. It is exactly what we expect from the CSM approach. As demonstrated in this paper, the method enables going down to the grain-grain size, all in reserving the possibility of analysis at sample scale.

Thanks to the cross-scales analysis, the results highlight that the macro shear band is associated with changes in micromechanics properties. The void ratio and micro-cracking increases from the zones outside SB to the adjacent zones and reaches maximum value in the core of SB. Setting an appropriate criterion for SB identification based on decohesion level of grains contacts or void ratio evolution are future directions of our research. Moreover, our cross-scale results demonstrate that the occurrence of SB is accompanied by increasing of void ratio and debonding at micro-scale.

Besides the advantages demonstrated in this article, the uncertainty of the CSM needs to be further explored as an interesting perspective. Since the VE composed of limited number of particles, preparing a series of similar VE (from

mechanical viewpoint) but with different grain sizes distribution as the one described in [22] would provide a more comprehensive and statistically meaningful view of the CSM. Moreover, it should be noted that only circular grains are used in the current CSM. To this end, irregular grain shape may be incorporated into DEM level of the CSM to better describe the rock materials.

Acknowledgements

This research is funded by Ministry of Education and Training under grant number B2023-XDA-09.

References

[1] Y. Abdallah, J. Sulem, M. Bornert, S. Ghabezloo, and I. Stefanou, (2021) *"Compaction banding in high-porosity carbonate rocks: 1. Experimental observations"* **Journal of Geophysical Research: Solid Earth *126***(1): e2020JB020538. DOI: 10.1029/2020JB020538.

[2] P. Bésuelle and J. W. Rudnicki, (2004) *"Localization: shear bands and compaction bands"* **INTERNATIONAL GEOPHYSICS SERIES. *89***: 219–322.

[3] M. Oda and K. Iwashita, (2000) *"Study on couple stress and shear band development in granular media based on numerical simulation analyses"* **International journal of engineering science *38***(15): 1713–1740. DOI: 10.1016/S0020-7225(99)00132-9.

[4] N. Estrada, A. Lizcano, and A. Taboada, (2010) *"Simulation of cemented granular materials. I. Macroscopic stress-strain response and strain localization"* **Physical Review E *82***(1): 011303. DOI: 10.1103/PhysRevE.82.011303.

[5] A. Ord, I. Vardoulakis, and R. Kajewski. "Shear band formation in Gosford sandstone". In: *International journal of rock mechanics and mining sciences & geomechanics abstracts*. ***28***. 5. Elsevier. 1991, 397–409. DOI: 10.1016/0148-9062(91)90078-Z.

[6] R. J. Finno, W. Harris, M. A. Mooney, and G. Viggiani, (1997) *"Shear bands in plane strain compression of loose sand"* **Geotechnique *47***(1): 149–165. DOI: 10.1680/geot.1997.47.1.149.

[7] H. Wu, N. Guo, and J. Zhao, (2018) *"Multiscale modeling and analysis of compaction bands in high-porosity sandstones"* **Acta Geotechnica *13***: 575–599. DOI: 10.1007/s11440-017-0560-2.

[8] P. Bésuelle, J. Desrues, and S. Raynaud, (2000) *"Experimental characterisation of the localisation phenomenon inside a Vosges sandstone in a triaxial cell"* **International Journal of Rock Mechanics and Mining Sciences *37***(8): 1223–1237. DOI: 10.1016/S1365-1609(00)00057-5.

[9] A. El Bied, J. Sulem, and F. Martineau, (2002) *"Microstructure of shear zones in Fontainebleau sandstone"* **International Journal of Rock Mechanics and Mining Sciences *39***(7): 917–932. DOI: 10.1016/S1365-1609(02)00068-0.

[10] J. Fonseca, P. Bésuelle, and G. Viggiani, (2013) *"Micromechanisms of inelastic deformation in sandstones: an insight using x-ray micro-tomography"* **Géotechnique Letters *3***(2): 78–83. DOI: 10.1680/geolett.13.034.

[11] P. Bésuelle. *"Déformation et rupture dans les roches tendres et les sols indurés: comportement homogène et localisation"*. (phdthesis). Université Joseph-Fourier-Grenoble I, 1999.

[12] P. Baud, V. Vajdova, and T.-f. Wong, (2006) *"Shear-enhanced compaction and strain localization: Inelastic deformation and constitutive modeling of four porous sandstones"* **Journal of Geophysical Research: Solid Earth *111***(B12): DOI: 10.1029/2005JB004101.

[13] M. P. Schöpfer and C. Childs, (2013) *"The orientation and dilatancy of shear bands in a bonded particle model for rock"* **International Journal of Rock Mechanics and Mining Sciences *57***: 75–88. DOI: 10.1016/j.ijrmms.2012.07.019.

[14] J. R. Rice and J. Rudnicki, (1980) *"A note on some features of the theory of localization of deformation"* **International Journal of solids and structures *16***(7): 597–605. DOI: 10.1016/0020-7683(80)90019-0.

[15] R. Chambon, S. Crochepeyre, and J. Desrues, (2000) *"Localization criteria for non-linear constitutive equations of geomaterials"* **Mechanics of Cohesive-frictional Materials: An International Journal on Experiments, Modelling and Computation of Materials and Structures *5***(1): 61–82.

[16] T. K. Nguyen, G. Combe, D. Caillerie, and J. Desrues, (2014) *"FEM× DEM modelling of cohesive granular materials: numerical homogenisation and multi-scale simulations"* **Acta Geophysica *62***: 1109–1126. DOI: 10.2478/s11600-014-0228-3.

[17] J. Desrues, A. Argilaga, D. Caillerie, G. Combe, T. K. Nguyen, V. Richefeu, and S. Dal Pont, (2019) *"From discrete to continuum modelling of boundary value problems in geomechanics: An integrated FEM-DEM approach"* **International Journal for Numerical and Analytical Methods in Geomechanics *43***(5): 919–955. DOI: 10.1002/nag.2914.

[18] P. A. Cundall and O. D. Strack, (1979) *"A discrete numerical model for granular assemblies"* **geotechnique *29***(1): 47–65. DOI: 10.1680/geot.1979.29.1.47.

[19] M. P. Allen and D. J. Tildesley. *Computer simulation of liquids*. Oxford university press, 2017.

[20] J.-Y. Delenne, M. S. El Youssoufi, F. Cherblanc, and J.-C. Bénet, (2004) *"Mechanical behaviour and failure of cohesive granular materials"* **International Journal for Numerical and Analytical Methods in Geomechanics *28***(15): 1577–1594. DOI: 10.1002/nag.401.

[21] T.-K. Nguyen, J. Desrues, T.-T. Vo, and G. Combe, (2022) *"FEM× DEM multi-scale model for cemented granular materials: Inter-and intra-granular cracking induced strain localisation"* **International Journal for Numerical and Analytical Methods in Geomechanics *46***(5): 1001–1025. DOI: 10.1002/nag.3332.

[22] T.-K. Nguyen. "On the Representative Volume Element of Dense Granular Assemblies Made of 2D Circular Particles". In: *Structural Health Monitoring and Engineering Structures: Select Proceedings of SHM&ES 2020*. Springer, 2021, 499–508.